SEC23B is required for the maintenance of murine professional secretory tissues

Jiayi Tao[a,1], Min Zhu[a,1], He Wang[b], Solomon Afelik[c], Matthew P. Vasievich[b], Xiao-Wei Chen[b], Guojing Zhu[b], Jan Jensen[c], David Ginsburg[b,d,2], and Bin Zhang[a,2]

[a]Genomic Medicine Institute, Lerner Research Institute, Cleveland Clinic Foundation, Cleveland, OH 44195; [b]Departments of Internal Medicine and Human Genetics, Life Sciences Institute, University of Michigan, Ann Arbor, MI 48109; [d]Howard Hughes Medical Institute, University of Michigan, Ann Arbor, MI 48109; and [c]Department of Stem Cell Biology and Regenerative Medicine, Lerner Research Institute, Cleveland Clinic Foundation, Cleveland, OH 44195

Contributed by David Ginsburg, May 31, 2012 (sent for review April 2, 2012)

In eukaryotic cells, newly synthesized secretory proteins require COPII (coat protein complex II) to exit the endoplasmic reticulum (ER). COPII contains five core components: SAR1, SEC23, SEC24, SEC13, and SEC31. SEC23 is a GTPase-activating protein that activates the SAR1 GTPase and also plays a role in cargo recognition. Missense mutations in the human COPII paralogues SEC23A and SEC23B result in craniolenticulosutural dysplasia and congenital dyserythropoietic anemia type II, respectively. We now report that mice completely deficient for SEC23B are born with no apparent anemia phenotype, but die shortly after birth, with degeneration of professional secretory tissues. In SEC23B-deficient embryonic pancreas, defects occur in exocrine and endocrine tissues shortly after differentiation. Pancreatic acini are completely devoid of zymogen granules, and the ER is severely distended. Similar ultrastructural alterations are also observed in salivary glands, but not in liver. Accumulation of proteins in the ER lumen activates the proapoptotic pathway of the unfolded protein response, suggesting a central role for apoptosis in the degeneration of these tissues in SEC23B-deficient embryos. Although maintenance of the secretory pathway should be required by all cells, our findings reveal a surprising tissue-specific dependence on SEC23B for the ER exit of highly abundant cargo, with high levels of SEC23B expression observed in professional secretory tissues. The disparate phenotypes in mouse and human could result from residual SEC23B function associated with the hypomorphic mutations observed in humans, or alternatively, might be explained by a species-specific shift in function between the closely related SEC23 paralogues.

mammalian embryo abnormalities | vesicular transport protein | genetics | secretory granules | pancreatitis

In eukaryotic cells, secreted proteins and proteins that are targeted to the plasma membrane and internal organelles are synthesized in the endoplasmic reticulum (ER) and sorted through the secretory pathway. This process has been extensively studied, particularly in budding yeast (1). Proteins destined to traffic from the ER to the Golgi are packaged into COPII (coat protein complex II)-coated vesicles (2–4). COPII is composed of at least five proteins, a small GTPase SAR1 and two cytosolic protein complexes, SEC23–SEC24 and SEC13–SEC31 (5). The GTP-bound form of SAR1 binds to the ER membrane and recruits the SEC23–SEC24 heterodimer to form the "prebudding complex," which in turn recruits the outer coat composed of SEC13–SEC31 heterotetramers to complete the COPII coat structure (6).

The COPII complex captures cargo into vesicles and mediates vesicle budding from the ER. Cargo recognition appears to be mediated primarily by the SEC24 subunit, which recognizes divergent export signals located in the cytosolic domain of cargo proteins (7, 8). SEC23 and SAR1 also play a role in the recognition of at least a subset of cargos (9, 10). SEC23 is a GTPase-activating protein (GAP) that activates the SAR1 GTPase (11). Conversion of SAR1-GTP to SAR1-GDP results in its dissociation from the COPII coat. Recent structural data revealed that the SAR1-bound SEC23 is in direct contact with the C terminus of SEC31, constituting a link between the outer-coat SEC13–SEC31 complex and the inner-coat SAR1–SEC23–SEC24 complex (12, 13). Interaction of SEC23 with the outer coat stimulates the GAP activity and accelerates the GTP hydrolysis of SAR1. After SAR1 release, SEC23 interacts with the TRAPPI complex subunits BET3 and dynactin, suggesting a function in vesicle tethering, fusion, and transportation along microtubules (14, 15). Finally, phosphorylation of SEC23 is thought to facilitate the fusion of COPII vesicles with the target membrane (16).

Mammalian cells express multiple paralogues of COPII proteins, including two SEC23 paralogues, SEC23A and SEC23B. Recently, two human genetic disorders have been associated with defects in *SEC23* genes. Craniolenticulosutural dysplasia (CLSD) is characterized by craniofacial and skeletal malformation resulting from homozygosity of missense mutations in SEC23A (17, 18). One of these mutations (F328L) interferes with the recruitment of SEC13–SEC31 to the prebudding complex, blocking COPII coat assembly and resulting in accumulation of secretory proteins in the ER lumen (18, 19). Skin fibroblasts from patients with CLSD exhibit defects in collagen secretion (17). Mutations in *SEC23B* were recently found to cause congenital dyserythropoietic anemia type II (CDAII) (20, 21). Patients with CDAII exhibit moderate anemia and multinucleated erythroblasts, ineffective erythropoiesis, and aberrant glycosylation of specific red blood cell membrane proteins. How SEC23B deficiency leads to this selective red blood cell defect in humans remains unclear.

Here we show that SEC23B deficiency leads to severe abnormalities in pancreas and other exocrine glands such as salivary and nasal glands, as well as glands in the digestive tract, during murine embryogenesis.

Results

SEC23B Deficiency Results in Perinatal Lethality in Mouse. PCR and sequence analysis of ES cell clone AD0407 identified the precise gene-trap insertion site in intron 19 of the murine *Sec23b* gene (Fig. 1*A* and Fig. S1). A three-primer PCR genotyping assay was used to differentiate the WT allele and the gene-trap allele (Fig. 1*B* and Fig. S1). Homozygous gene-trap mice were generated from intercrosses of mice backcrossed at least eight generations (i.e., N8) into the C57BL/6J background or the 129/SvImJ

Author contributions: D.G. and B.Z. designed research; J.T., M.Z., H.W., S.A., M.P.V., X.-W.C., G.Z., and B.Z. performed research; J.J., D.G., and B.Z. analyzed data; and J.T., M.Z., D.G., and B.Z. wrote the paper.

The authors declare no conflict of interest.

[1]J.T. and M.Z. contributed equally to this work.

[2]To whom correspondence may be addressed. E-mail: ginsburg@umich.edu or zhangb@ccf.org.

See Author Summary on page 11478 (volume 109, number 29).

This article contains supporting information online at www.pnas.org/lookup/suppl/doi:10.1073/pnas.1209207109/-/DCSupplemental.

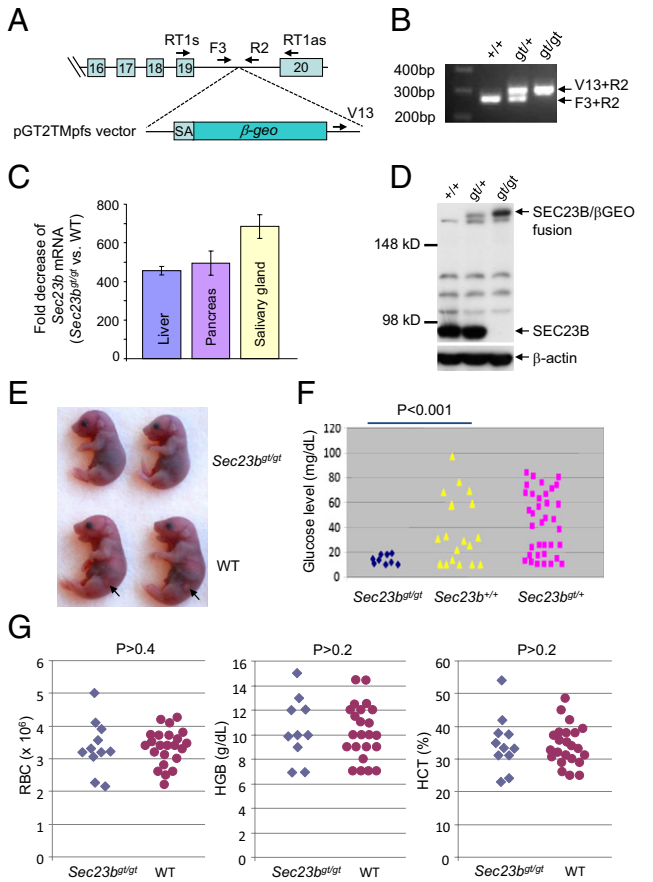

Fig. 1. Generation of SEC23B-deficient mice. (*A*) Insertion of the gene-trap cassette within intron 19 of the *Sec23b* genomic locus results in a cDNA fusion of the first 19 exons with the *β-Geo* gene from the gene-trap vector (pGT2TMpfs). Locations of the RT-PCR and genotyping primers are indicated. SA, splice acceptor. (*B*) A three-primer genotyping assay distinguishes all three genotypes. Locations of the genotyping primer sequences are indicated in Fig. S1 and *A*. (*C*) Real-time RT-PCR analysis of *Sec23b* mRNA from total RNA prepared from liver, pancreas, and salivary glands of three E14.5 embryos of each genotype. The fold decreases in $Sec23b^{gt/gt}$ vs. WT mice are plotted. gt, gene trap. Error bars represent SDs. (*D*) Western blot analysis demonstrating the absence of WT SEC23B protein from $Sec23b^{gt/gt}$ MEFs and the presence of SEC23B/βGEO fusion protein by using a SEC23B-specific antibody. (*E*) $Sec23b^{gt/gt}$ neonates are consistently smaller than their WT littermates. Arrows denote the pancreatic tissue visible from the left side of WT pups but not evident in $Sec23b^{gt/gt}$ pups. (*F*) Blood glucose levels in WT, $Sec23b^{gt/+}$, and $Sec23b^{gt/gt}$ pups. Results were obtained from natural or cesarean section-born pups that were fasted for 4 to 8 h before testing. (*G*) Normal peripheral blood counts in $Sec23b^{gt/gt}$ mice. Red blood cell (RBC) count and hemoglobin (HGB) and hematocrit (HCT) levels are not significantly different between WT and $Sec23b^{gt/gt}$ pups.

background. The gene trap is predicted to produce an N-terminal protein fragment encoded by the first 19 exons of *Sec23b* fused to the *β-Geo* (β-gal and neomycin phosphotransferase fusion gene) protein product. This fusion deletes the C-terminal 29 aa of SEC23B. To assess the efficiency of exon 19 splicing to the gene-trap insert, total RNA was isolated from tissues of mice homozygous for the gene-trap allele ($Sec23b^{gt/gt}$) as well control mice ($Sec23b^{+/+}$). Real-time RT-PCR was performed by using primers that span the exon 19–20 junction. The amount of WT *Sec23b* transcript in $Sec23b^{gt/gt}$ cells is reduced more than 400-fold compared with the WT transcript (Fig. 1*C*). Immunoblot analysis also failed to detect WT SEC23B protein in $Sec23b^{gt/gt}$ mouse embryonic fibroblasts (MEFs; Fig. 1*D*). However, the expected SEC23B/βGEO fusion protein derived from the gene-trap allele is evident in $Sec23b^{gt/+}$ and $Sec23b^{gt/gt}$ cells (Fig. 1*D*). Both SEC23B and this fusion protein coimmunoprecipitated with SEC24A in MEF lysates (Fig. S2).

Although $Sec23b^{gt/gt}$ pups were born alive, they failed to suckle and generally died within hours of birth, with none surviving beyond 24 h. Timed matings revealed close to expected number of $Sec23b^{gt/gt}$ embryos at E18.5 and earlier time points during embryogenesis (Table 1), indicating that the majority of null embryos survive to term. $Sec23b^{gt/gt}$ pups delivered through cesarean section at E18.5 were alive but generally died within 12 h after birth (the end point of observation). Body weight of $Sec23b^{gt/gt}$ neonates ($n = 19$) is ~25% lower ($P < 0.001$) than their WT ($n = 23$) and $Sec23b^{gt/+}$ ($n = 40$) littermates, but otherwise showed no gross abnormalities (Fig. 1*E*). Heterozygous mice appeared normal and exhibited normal survival and fertility. $Sec23b^{gt/gt}$ mice backcrossed at least eight generations on the C57BL/6J or 129/SvImJ strain background appear grossly similar, with similar neonatal mortality (Table 1). Subsequent analyses were restricted to $Sec23b^{gt/gt}$ mice (backcrossed at least eight generations) on C57BL/6J background.

Hypoglycemia with No Apparent Anemia and Skeletal Development Defect in $Sec23b^{gt/gt}$ Neonates. Neonatal blood glucose levels were measured at 4 to 8 h after birth under nonsuckling conditions, at which point maternal-derived glucose should be replaced by glucose generated by the pups (22). Approximately 70% of $Sec23b^{+/+}$ and $Sec23b^{gt/+}$ neonates exhibited glucose concentrations greater than 20 mg/dL. In contrast, all nine $Sec23b^{gt/gt}$ mice had glucose levels <20 mg/dL ($P < 0.001$; Fig. 1*F*).

Mutations in *SEC23B* cause CDAII in humans (20, 21). However, no significant differences in red blood cell count, hemoglobin, or hematocrit levels were observed in blood collected from WT and $Sec23b^{gt/gt}$ neonates (Fig. 1*G*). Mutations in SEC23A result in abnormalities of cartilage and bone development in humans and zebrafish (18, 23). Although E18.5 $Sec23b^{gt/gt}$ neonates are smaller than WT controls, no skeletal abnormalities were evident by Alcian blue/alizarin red staining (Fig. S3). In addition, $Sec23b^{gt/gt}$ MEFs showed no abnormality in the intracellular localization or secretion of collagen I (Fig. S4*A*). Staining with markers for ER (protein disulfide isomerase), ER exit sites (SEC13), and ER–Golgi intermediate compartment (LMAN1) revealed no obvious differences between WT and $Sec23b^{gt/gt}$ MEFs (Fig. S3 *B* and *C*).

SEC23B Deficiency Results in Impaired Pancreatic Development. Compared with WT controls, the volume of the dorsal and ventral pancreas was markedly decreased in $Sec23b^{gt/gt}$ pups (Fig. 2*A*), with a more opaque appearance (Fig. 1*E*). H&E and immunostaining showed a disorganized structure in the $Sec23b^{gt/gt}$ pancreas (Fig. 2*B*). Cytokeratin staining revealed a consistent decrease in the size and number of pancreatic acini. The typical

Table 1. Genotype distribution of embryos and pups from intercrosses of $Sec23b^{gt/+}$ mice

Background	*Sec23b* genotype			*P* value
	$^{+/+}$ (%)	gt/$^{+}$ (%)	gt/gt (%)	
E18.5 (n = 154), C57BL/6J	45 (29.2)	78 (50.7)	31 (20.1)	>0.2
E16.5 (n = 81), C57BL/6J	19 (23.5)	47 (58)	15 (18.5)	>0.2
E15.5 (n = 142), C57BL/6J	33 (23.2)	75 (52.8)	34 (24)	>0.7
E14.5 (n = 103), C57BL/6J	28 (27.2)	59 (57.3)	16 (15.5)	>0.08
E13.5 (n = 64), C57BL/6J	15 (23.4)	34 (53.1)	15 (23.4)	>0.8
Weaning (n = 57), C57BL/6J	18	39	0	—
Weaning (n = 44), 129/SvImJ	13	31	0	—

Mice were backcrossed at least eight generations into the C57BL/6J or 129/SvImJ background.

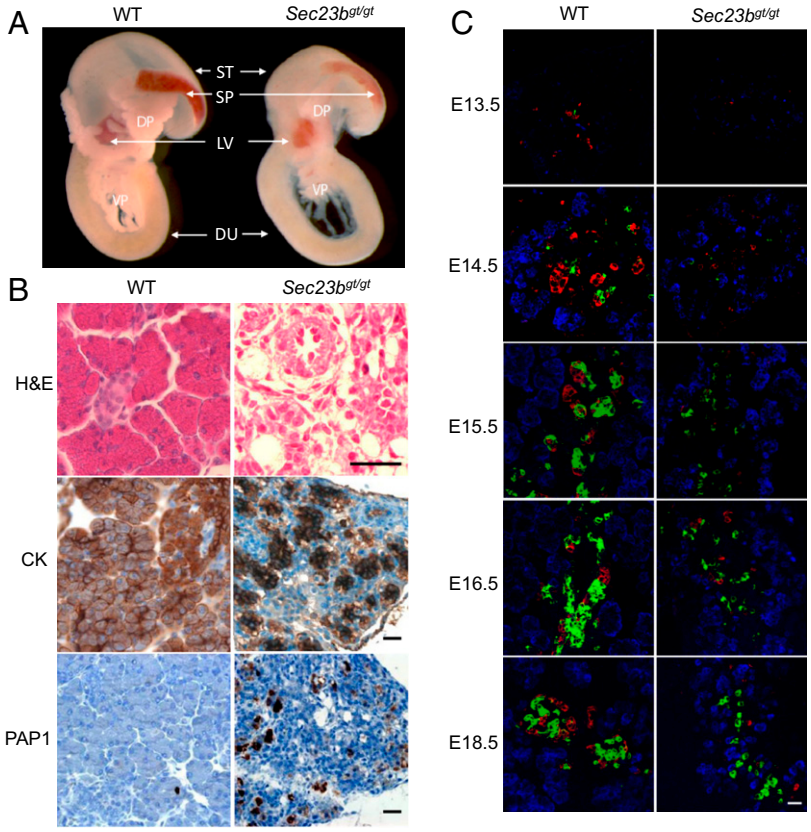

Fig. 2. Pancreatic defect in *Sec23b*$^{gt/gt}$ mice. (*A*) Pancreas and adjacent tissues dissected from E18.5 embryos. Pancreatic tissues from *Sec23b*$^{gt/gt}$ embryos are smaller and less demarcated than in WT embryos. DP dorsal pancreas; DU, duodenum; LV, liver; SP, spleen; ST, stomach; VP, ventral pancreas. (*B*) H&E and immunohistochemical staining of pancreas from WT and *Sec23b*$^{gt/gt}$ mice. PAP1, pancreatitis associated protein 1; CK, cytokeratin. (Scale bar: 30 μm.) (*C*) Immunofluorescence staining of pancreas at E13.5, E14.5, E15.5, E16.5, and E18.5. Cryosections were costained with rabbit anti-carboxylpeptidase A (blue) for exocrine cells and mouse anti-glucagon (red) and guinea pig anti-insulin (green) for α- and β-endocrine cells, respectively. (Scale bar: 25 μm.)

grape-like clusters of acinar cells of the WT pancreas are lost in *Sec23b*$^{gt/gt}$, with no discernible islet structure (Fig. 2*B*). Positive staining for PAP1 (pancreatitis-associated protein 1) in the *Sec23b*$^{gt/gt}$ pancreas (Fig. 2*B*) suggests inflammation associated with the observed pancreatic degeneration.

Immunofluorescence staining for carboxypeptidase A (CPA), an acinar cell marker, and for the endocrine cell markers insulin (β-cells) and glucagon (α-cells), demonstrated a striking difference in the distribution pattern of endocrine cells as early as E13.5, and more pronounced at later time points (E14.5, E15.5, E16.5 and E18.5; Fig. 2*C*). At E18.5, α- and β-cells in the WT pancreas have migrated to form the islets of Langerhans, represented by a structure in which insulin-positive β-cells cluster in the core and glucagon-positive α-cells cluster at the periphery. By contrast, both α- and β-cells are markedly reduced in number and remain scattered in the *Sec23b*$^{gt/gt}$ pancreas throughout development (Fig. 2*C*).

The defects in exocrine and endocrine compartments of the *Sec23b*$^{gt/gt}$ pancreas prompted us to examine if this reflects an essential role of SEC23B in early stages of pancreas development. Immunofluorescence analysis of the embryonic pancreas at embryonic day (E) 13.5, just before terminal differentiation, revealed no apparent defects in pancreatic progenitor cells as marked by the expression of Pdx1 in *Sec23b*$^{gt/gt}$ (Fig. 3). During branching morphogenesis, the pancreas is prepatterned into proacinar and proendocrine/ductal progenitor domains, which are localized to the "tip" and "trunk" of the branched epithelial network, respectively (24). By using the tip marker Ptf1a and the trunk-specific progenitor marker Nkx6.1 (25, 26), we find that the *Sec23b*$^{gt/gt}$ embryonic pancreas undergoes normal prepatterning to generate proacinar and proendocrine/ductal progenitor cells (Fig. 3). Furthermore, endocrine progenitor cells are appropriately specified within the trunk domain, as marked by the normal expression of Ngn3 (Fig. 3), a key transcription factor for the development of all endocrine cells in the pancreas (27, 28). Taken together, we conclude that the loss of endocrine and exocrine cells in *Sec23b*$^{gt/gt}$ pancreas is not the result of defective pancreatic progenitor fate assignment.

SEC23B-Deficient Pancreatic Acinar Cells Lack Zymogen Granules and Accumulate Exocrine Proteins in ER Lumen. Pancreatic cell ultrastructure was further examined by transmission EM. In developing pancreas, acinar protein expression begins at E13.5. By E16.5, most WT acinar cells have accumulated large numbers of zymogen granules. However, no zymogen granules are seen in *Sec23b*$^{gt/gt}$ acini at E16.5 (Fig. 4*A*). Compared with the normal cisternae structure of the rough ER in WT acini, distended ER was observed in a minority of acinar cells in the *Sec23b*$^{gt/gt}$ E13.5 pancreas (Fig. 4*A*). By E16.5, grossly distended ER is seen in a majority of *Sec23b*$^{gt/gt}$ acinar cells. Of note, those cells that exhibit normal ER structures also contain no zymogen granules, suggesting that these morphologically normal cells are not actively synthesizing large amounts of zymogens.

Abnormal distribution of acinar proteins is detected in immunofluorescence staining for CPA, which shows perinuclear clustering in *Sec23b*$^{gt/gt}$ acinar cells, in contrast to the peripheral cytoplasmic staining in WT acinar cells (Fig. 4*B*). Similar patterns were also observed in experiments with anti-amylase an-

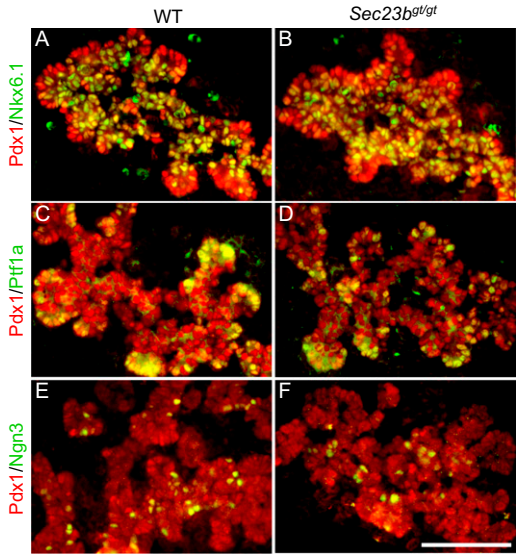

Fig. 3. Immunofluorescence staining of pancreas at E13.5 for pancreatic progenitor markers. Cryosections were costained with Pdx1 for all pancreatic progenitor cells (red) and the proendocrine/duct progenitor marker Nkx6.1 (*A* and *B*), the proacinar progenitor maker Ptf1a (*C* and *D*), and the endocrine progenitor marker Ngn3 (*E* and *F*), all in green. (Scale bar: 50 μm.)

tibody. We used immuno-EM to further analyze the subcellular distribution of amylase and glucagon. In WT acinar cells, anti-amylase gold particles are concentrated in the zymogen granules (Fig. 4*B*). In *Sec23b*$^{gt/gt}$ acinar cells, gold particles were detected in the dilated ER lumen, consistent with the accumulation of proamylase and other exocrine proteins in the ER. The different localization patterns observed in the immunofluorescence staining of CPA therefore reflect the difference in its localization between zymogen granules (in WT) and the distended ER (in *Sec23b*$^{gt/gt}$). In WT α-cells stained with anti-glucagon, gold particles are concentrated in secretory granules as expected (Fig. 4*B*). Consistent with the markedly decreased insulin and glucagon positive cells by immunofluorescence staining (Fig. 2*C*), cells with gold particle-positive granules were only rarely found in *Sec23b*$^{gt/gt}$ pancreas (at most two α-cells were found in a whole cross-section of *Sec23b*$^{gt/gt}$ dorsal pancreas, whereas more than 40 α-cells were observed in the WT section). However, granules observed in these rare cells appear normal in morphology (Fig. 4*B*). Taken together, our data suggest that SEC23B deficiency inhibits the ER exit of exocrine proteins in pancreatic acinar cells.

Impaired Development of Other Secretory Tissues in SEC23B-Deficient Mice. In addition to pancreas, we identified degeneration of other exocrine tissues, including salivary and nasal glands, as well as glands in the stomach and intestines, in E18.5 embryos (Fig. 5*A*). The structures of serous and mucous acini of salivary glands are disrupted, reminiscent of the phenotype observed for pancreatic acini (Fig. 2*B*). The morphology of other secretory tissues, such as the gastric epithelium, gastric glands, nasal glands, goblet cells, and Paneth cells in intestinal crypts are also perturbed (Fig. 5*A* and Fig. S5). In contrast, thymus and thyroid glands are grossly normal in *Sec23b*$^{gt/gt}$ embryos (Fig. S5). The effect of SEC23B deficiency on the ultrastructure of salivary gland cells was further analyzed by transmission EM on ultrathin sections of E18.5 salivary glands. In WT embryos, serous acini in sublingual gland and mucous acini in submandibular gland contain secretory granules and normal ER structure (Fig. 5*B*). In contrast, mucous and serous acini in *Sec23b*$^{gt/gt}$ embryos contain grossly dilated ER. In contrast to the pancreatic acinar cells, a small percentage of *Sec23b*$^{gt/gt}$ serous acinar cells still contain secretory granules, albeit in much reduced numbers compared with WT (on average, a reduction to ~15% of WT level), with no secretory granules evident in *Sec23b*$^{gt/gt}$ mucous acini (Fig. 5*B*).

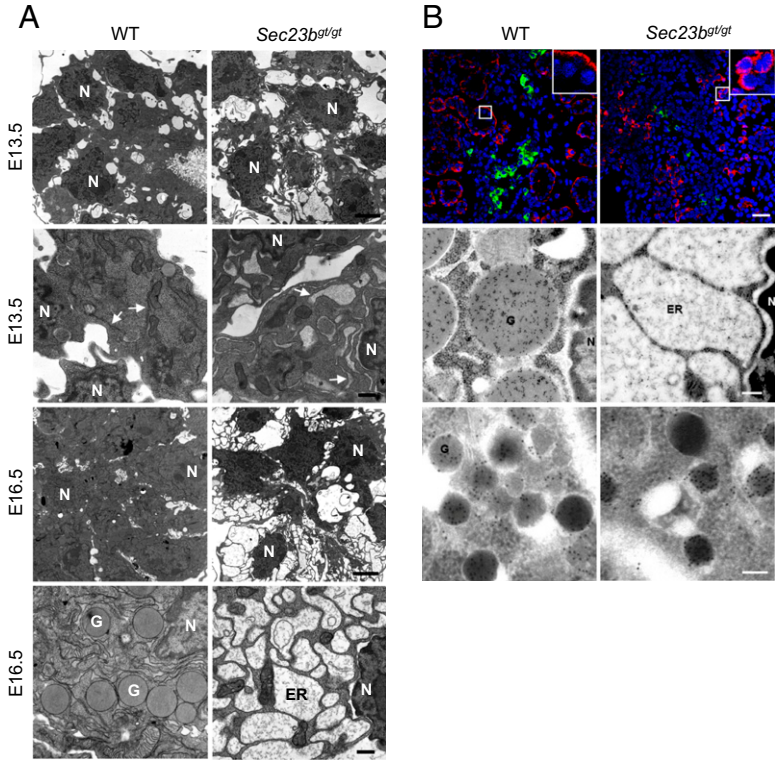

Fig. 4. Abnormal ER structure and accumulation of proteins in the ER lumen. (*A*) EM shows the lack of zymogen granules and the grossly distended ER in *Sec23b*$^{gt/gt}$ pancreatic acinar cells. Thin sections prepared from WT control and *Sec23b*$^{gt/gt}$ pancreas from E13.5 and E16.5 embryos were observed and imaged on a transmission electron microscope. Dilated ER structure was detected as early as E13.5 in null acinar cells. These ER changes became more severe at E16.5. Arrows indicate ER. G, granule; N, nucleus. (Scale bars: lower magnification, 3 μm; higher magnification, 0.5 μm.) (*B*) *Top*: Immunofluorescence staining of pancreas at E18.5 with CPA (red), insulin (green), and DAPI (blue nuclei) indicates a change in localization pattern of exocrine proteins. Top right corner contains magnified image from the boxed region. Signals of CPA cluster in juxtanuclear position in *Sec23b*$^{gt/gt}$ pancreas, whereas it is found in the outer cytoplasm in WT controls. (Scale bar: 25 μm.) *Middle*: immunogold staining of amylase. In WT acini, gold particles are specifically enriched in zymogen granules, whereas, in SEC23B-null acinar cells, particles are scattered in the distended ER lumen. (Scale bar: 0.2 μm.) *Bottom*: Immunogold staining of glucagon. Gold particle-positive α-cells are readily detected in WT pancreas, but rarely found in *Sec23b*$^{gt/gt}$ pancreas. G, granule; N, nuclear. (Scale bar: 0.1 μm.).

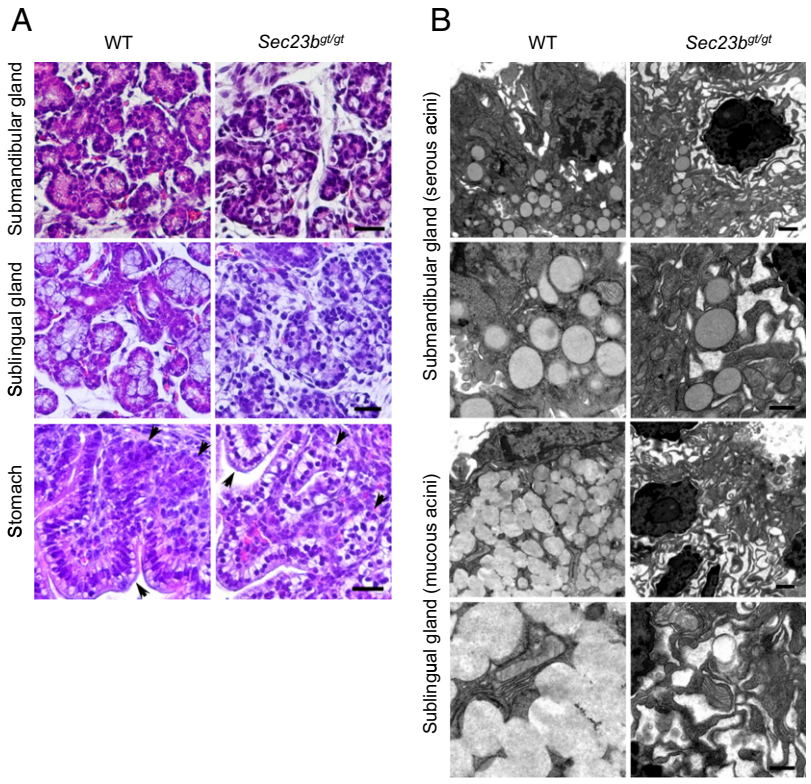

Fig. 5. Defective exocrine glands in *Sec23b*$^{gt/gt}$ mice. (*A*) H&E staining of submandibular gland, sublingual gland and the fundus of stomach of WT and *Sec23b*$^{gt/gt}$ E18.5 embryos. Arrows denote gastric epithelium and gastric glands in stomach. Degeneration of serous and mucous acini and the gastric glands is evident with the disorganized structures and abundance of unstained intracellular spaces in *Sec23b*$^{gt/gt}$ embryos. (Scale bar: 50 μm.) (*B*) EM images of serous acini and mucous acini in salivary glands of WT and *Sec23b*$^{gt/gt}$ E18.5 embryos. Dilated ER structure is observed in both types of acini, with no secretory granules found in mucous acini in *Sec23b*$^{gt/gt}$ E18.5 salivary glands. (Scale bars: lower magnification, 1 μm; higher magnification, 0.5 μm.)

To rule out the possibility that the phenotype observed in *Sec23b*$^{gt/gt}$ mice is a result of residual functional activity from the SEC23B/βGEO fusion protein, or changes at another locus resulting from a passenger gene mutation (29), we generated a second SEC23B-deficient mouse line from another ES cell clone carrying a floxed *Sec23b* KO allele and a gene-trap insertion in intron 4 (Fig. S6). Mice homozygous for the second gene-trap alleles (*Sec23b*$^{gt2/gt2}$) show a similar neonatal lethality (with no *Sec23b*$^{gt2/gt2}$ neonates surviving past day 1) and degeneration of pancreas, salivary, gastric, and nasal glands (Fig. S7). Deletion of the floxed exons 5 and 6 from these mice also produced the same phenotype.

SEC23B Deficiency Leads to Apoptosis of Secretory Tissues in Developing Embryo. To determine whether the distended ER and accumulation of proteins in the ER lumen in *Sec23b*$^{gt/gt}$ secretory tissues is associated with the induction of ER stress and the unfolded protein response (UPR), expression levels for representative UPR genes were measured in the pancreas and submandibular glands by real-time PCR. Liver, also a highly secretory organ, appears to contain ER with normal structure (Fig. S8), but was also included in the mRNA analysis. Expression of the proapoptotic transcription factor *Chop* (*Gadd153*) and its downstream target *Trb3*, is markedly up-regulated in pancreas from *Sec23b*$^{gt/gt}$ embryos at E14.5 and E18.5, whereas genes in the adaptive UPR pathway are down-regulated, including the ER chaperone *Grp78*, alternatively spliced transcription factor *Xbp1*, and ER-associated degradation component *Edem1* (Fig. 6*A*) (30, 31). In submandibular glands, whereas *Chop*, *Trb3*, and *Gadd34* are progressively up-regulated from E14.5 to E18.5, expression of adaptive genes such as *Grp78* is also elevated, in contrast to the down-regulation observed in the pancreas (Fig. 6*A*). These findings are consistent with the less severe destruction of the serous acini observed in Fig. 5*B*. In the embryonic liver, although *Chop* and *Trb3* are transiently up-regulated at E14.5, most UPR genes show no difference in expression between WT and *Sec23b*$^{gt/gt}$, consistent with the normal histology in *Sec23b*$^{gt/gt}$ liver (Fig. S8).

Immunofluorescence staining of activated caspase-3 was performed on frozen sections of E18.5 embryos. Results demonstrated a significant increase in the number of caspase-3–positive cells in pancreas, salivary gland, and gastric glands in *Sec23b*$^{gt/gt}$ embryos (Fig. 6*B*). Furthermore, TUNEL staining of embryos at different time points revealed that the apoptotic cells start to appear in pancreas at E15.5 (Fig. S9*A*), whereas no TUNEL-positive cells are detectable at this time point in salivary glands (Fig. S9*B*). These results indicate that increased apoptosis occurs after cells start to synthesize large amount of secretory cargo.

Comparison of Expression Profiles for Murine SEC23A and SEC23B. To assess relative expression at the protein level for SEC23A and SEC23B, Western blot analysis was performed in cell lysates prepared from dissected organs of WT E18.5 embryos by using anti-SEC23A and anti-SEC23B antibodies, as well as an antibody that recognizes both paralogues (Fig. 7*A*). SEC23A and SEC23B are both widely expressed, with considerable variation among tissues. SEC23B protein appears to be most abundant in the pancreas and salivary glands, with lower levels in brain and heart. Pancreas and salivary glands also express relatively low levels of SEC23A compared with other tissues, with relatively high levels of SEC23A observed in brain, intestine, and yolk sac. The gene trap allele produces a SEC23B and β-GEO fusion

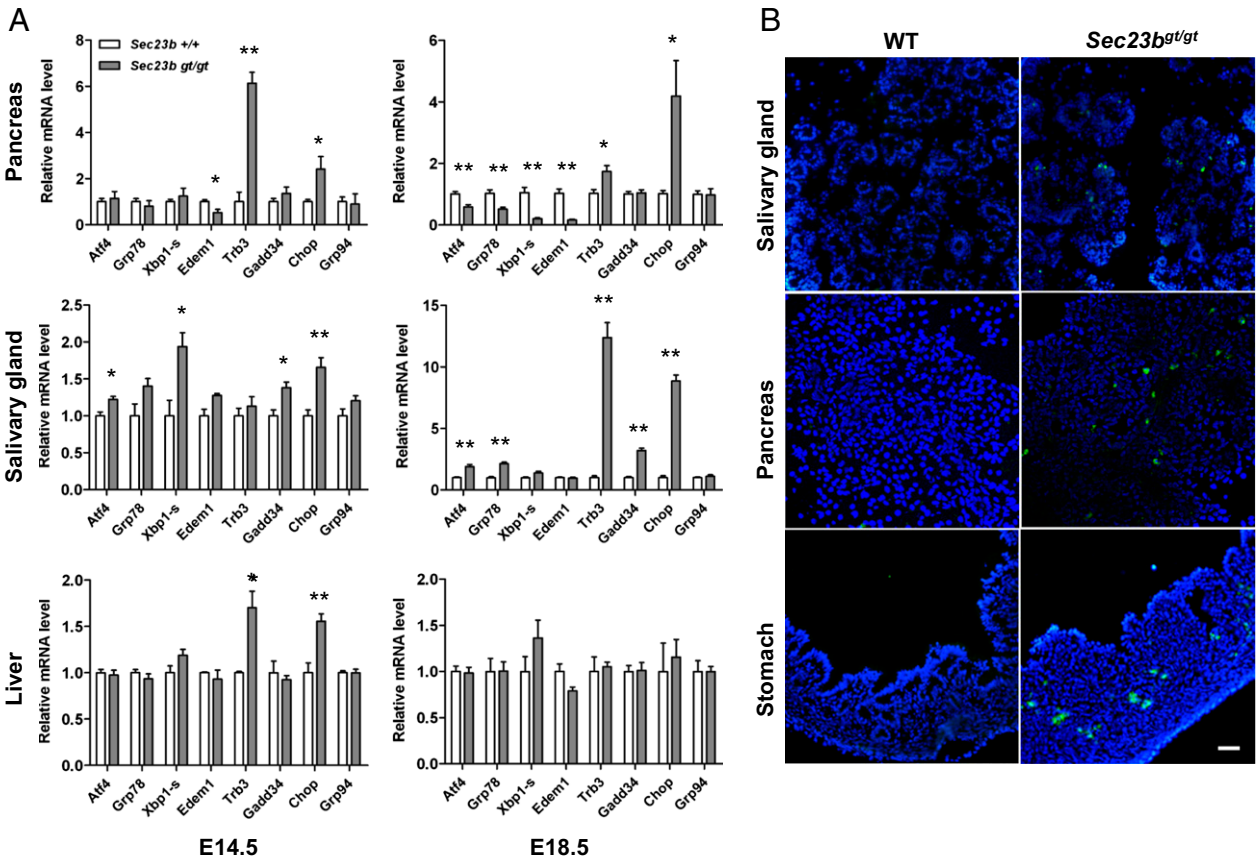

Fig. 6. Expression of UPR genes in developing pancreas and salivary glands. (*A*) Real-time RT-PCR quantification was performed for expression of select UPR genes in E14.5 and E18.5 pancreas, submandibular salivary gland, and liver samples. *Chop*, *Gadd34*, and *Trb3* are genes in the proapoptotic pathway, whereas other genes primarily act in the adaptive pathways. Expression of the β-actin gene was used as reference. Data are mean ± SEM. Asterisks indicate statistically significant differences between WT and *Sec23b*$^{gt/gt}$ samples (*$P < 0.05$ and **$P < 0.01$, Student *t* test). (*B*) Increased apoptosis in *Sec23b*$^{gt/gt}$ tissues. Immunofluorescence staining for activated caspase-3 was performed on cryosections of E18.5 pancreas, fundus of stomach, and submandibular gland. Caspase-3–positive cells are visualized in green, and nuclei are stained blue with DAPI. (Scale bar: 100 μm.)

protein driven by the *Sec23b* promoter (Fig. 1). Therefore, β-gal activity is a proxy for endogenous *Sec23b* gene expression. X-gal staining was conducted to characterize the detailed expression patterns of SEC23B in select organs. The *Sec23b* gene appears to be expressed predominantly in acinar cells of both pancreas and salivary glands (with higher expression in sublingual gland than submandibular gland), as well as in pancreatic islet cells, with much lower expression in other cell types such as duct cells. In the stomach, *Sec23b* gene expression is seen predominantly in the epithelium and gastric glands in the stomach, but not in the lamina propria and smooth muscle cells (Fig. 7*B*).

We further estimated the relative expression levels of the two SEC23 paralogues in the same tissues and cells (Fig. 7*C*). Steady-state SEC23B protein levels are notably higher than SEC23A in pancreas (approximately ninefold) and salivary gland lysates (approximately sixfold), as well as in lysates prepared from α- (approximately eightfold) and β- (approximately twofold) cell lines (Fig. 7*C*). In contrast, SEC23A is expressed at higher levels than SEC23B in the liver (Fig. 7*C*).

Discussion

We have demonstrated that complete SEC23B deficiency in the mouse results in severe developmental defects in the pancreas and other exocrine glands. Exocrine and endocrine structures in the pancreas are severely disrupted, with no secretory granules identified in acinar cells, a marked decrease in endocrine cell number, and the absence of typical islet structure. The normal number of progenitor cells in *Sec23b*$^{gt/gt}$ embryos suggests that the observed defects in exocrine and endocrine cells occur after their differentiation. Hypoglycemia in newborn *Sec23b*$^{gt/gt}$ mice, perhaps as a result of an imbalance in insulin and glucagon secretion, may be the cause of death in most *Sec23b*$^{gt/gt}$ pups. Mice completely lacking a pancreas are also smaller and die a few days after birth (32). However, failure to suckle suggests the presence of other abnormalities not evident on gross morphologic analysis. Pups that survived hypoglycemia may eventually die of dehydration.

The gene-trap allele is likely a null allele as it produces a β-GEO fusion protein that deletes the C-terminal sequence of SEC23B, which binds to SAR1 (33) and is also the target of phosphorylation by a casein kinase, a step required for COPII vesicle fusion with the pre-Golgi (16). The identification of a human CDAII mutation (H757P) within this deleted C-terminal segment of SEC23B is also consistent with the importance of this domain for SEC23B function (34). Although the fusion protein does retain some interaction with SEC24A (Fig. S5), SAR1 binding defect and steric hindrance by the β-GEO moiety may prevent assembly of the fusion protein into the COPII cage (12, 13). A dominant-negative function of the fusion protein also seems unlikely, given the lack of phenotype in heterozygous mice. Finally, the observation of the same neonatal lethality and secretory tissue phenotype in a second, independent SEC23B-deficient mouse lines with a gene trap in intron 4 and a third line with deletion of exons 5 and 6 indicates that the observed phenotype results solely from the loss of SEC23B function.

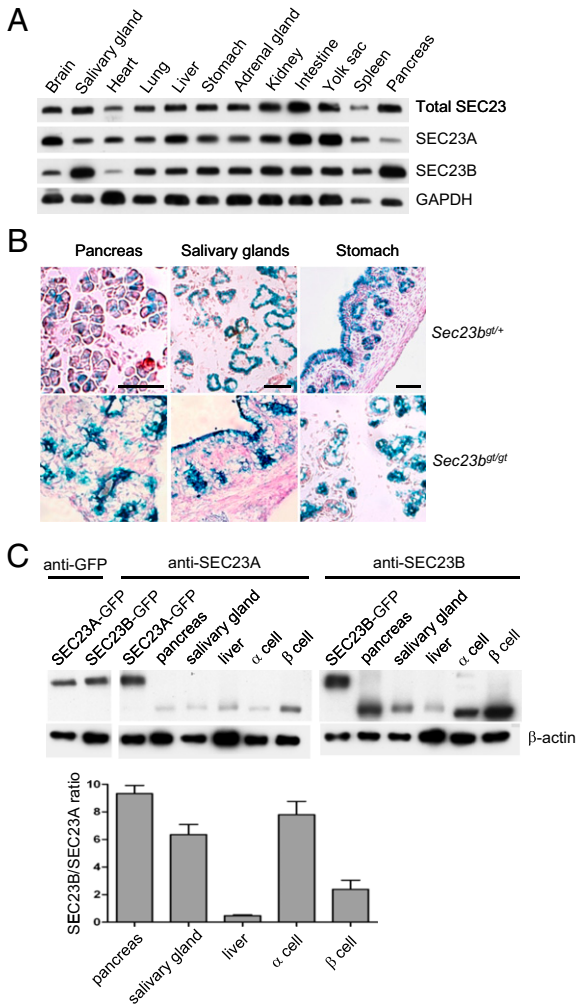

Fig. 7. Relative abundance of SEC23A and SEC23B across tissues of WT mice. (*A*) Lysates were prepared from E18.5 embryos and analyzed by Western blotting. Total SEC23 was detected by an antibody that recognizes both paralogues, whereas SEC23A and SEC23B were detected by specific antibodies. GAPDH serves as a loading control. (*B*) β-Gal staining of *Sec23b*$^{gt/+}$ and *Sec23b*$^{gt/gt}$ pancreas, salivary glands, and stomach from E18.5 embryos. For salivary glands, the lower left side of the image shows serous acini and the upper right side shows mucous acini. (Scale bar: 50 μm.) (*C*) Relative expression levels of SEC23A and SEC23B in the same tissues or cells. Levels of exogenously expressed GFP-SEC23A and GFP-SEC23B fusion proteins were first quantified by Western blot analysis by using an anti-GFP antibody (*Left*). Similar amounts of GFP-SEC23A and GFP-SEC23B proteins, along with lysates from E18.5 mouse embryonic pancreas, salivary gland, and liver, as well as lysates from α-TC1 β-TC-6 cells (American Type Culture Collection) were separated on single SDS/PAGE gels (*Right*). Western blot analysis was performed with antibodies specific for SEC23A or SEC23B. β-Actin was used as an internal control. The lower graph shows the quantitative comparison. Error bars represent mean ± SEM of results from three independent biological samples.

Of particular note, murine SEC23B deficiency does not recapitulate the anemia phenotype observed in human patients with CDAII. In addition, pancreatitis or dysfunction of other exocrine glands has not previously been reported in patients with CDAII. Given the early death of *Sec23b*$^{gt/gt}$ mice, we cannot exclude the possibility that significant anemia might have become evident after birth or was being masked by dehydration in the neonate. In addition, all patients with CDAII reported to date carry at least one missense allele (20, 21, 34, 35), suggesting that complete SEC23B deficiency might also be lethal in humans. The more severe clinical phenotype reported in patients with compound heterozygosity for a missense and nonsense mutation compared with those with two missense alleles (34, 35) is also consistent with this hypothesis.

Although the phenotype observed in SEC23B-deficient mice seems to arise predominantly through the disruption of function in professional secretory tissues in exocrine glands, liver and other highly secretory cell types do not appear to be as severely affected. The late lethality of SEC23B deficiency in mice, together with the survival of humans with at least partial deficiency of SEC23A or SEC23B, is surprising given the absolute requirement for Sec23 expression in yeast (36). This discrepancy is likely explained by an overlap in function and/or complementary expression programs for the two Sec23 paralogues found in mammals, in contrast to the single *Sec23* gene in yeast. Our observation of particularly high levels of SEC23B and comparably low levels of SEC23A in the pancreas and other secretory tissues is consistent with this model. SEC23B may be particularly critical to support the high secretory burden of these tissues, or to accommodate specific cargoes unique to these cell types. SEC23 is a GAP that promotes the conversion of SAR1-GTP to SAR1-GDP. Perhaps differential activity between SEC23B and SEC23A toward the two mammalian SAR1 proteins (37) could contribute to varied requirements for the two SEC23 paralogues among secretory cargoes.

Missense mutations in SEC23A cause CLSD and have been shown to disrupt collagen transport from ER to Golgi, providing a molecular mechanism for the mild skeletal deformation characteristic of this disorder (17, 18). Consistent with the human phenotype, the *Sec23a* mutant zebrafish (*crusher*) also exhibits abnormal cartilage development (23). However, knockdown of either *Sec23* isoform in zebrafish induced a phenotype similar to *crusher*, suggesting that zebrafish SEC23B may also be involved in cartilage maturation (23). A *Caenorhabditis elegans Sec23* mutant also exhibits defective secretion of the DPY-7 collagen gene (38). The absence of skeletal abnormalities in SEC23B-deficient neonates and lack of evidence for retention of collagen I in the ER of *Sec23b*$^{gt/gt}$ MEFs suggest that mammalian SEC23B may not contribute to collagen secretion and bone development, or that its role is largely compensated by SEC23A.

Accumulation of unfolded proteins in the ER lumen results in ER stress. The UPR is particularly important for maintaining normal function of the pancreas (39, 40). Low levels of ER stress primarily activate the adaptive UPR pathways (30, 31), as we observed in the liver of E18.5 *Sec23b*$^{gt/gt}$ embryos. In contrast, with persistent and severe ER stress, as seen in the E18.5 pancreas and salivary glands, the apoptosis is preferentially activated, likely through the PERK pathway (31). In addition to ER stress-induced apoptosis, zymogens released from dead cells may become activated, contributing to the degeneration of the affected organs. Autodigestion associated with increased trypsin activity underlines familial chronic pancreatitis (41). In addition, ER stress-induced apoptosis was observed in exocrine tissues carrying a pancreatitis-associated chymotrypsinogen C mutation (42). Taken together with these earlier findings, our observation that the exocrine cells of the pancreas are particularly sensitive to SEC23B deficiency suggests a previously unappreciated role for abnormalities in ER-to-Golgi transport in the pathogenesis of pancreatitis.

Materials and Methods

Generation of SEC23B-Deficient Mice. An ES cell clone (AD0407) with a gene-trap insertion in intron 19 of the *Sec23b* gene was obtained from the International Gene Trap Consortium. The ES cell clone was expanded, correct targeting was confirmed by RT-PCR, and it was then injected into C57BL/6J blastocysts by the transgenic mouse core at the University of Michigan. Germ-line transmission of the mutant allele was achieved by mating chimeric founders with C57BL/6J mice or with 129/SvImJ mice. The gene-trap

allele was continuously backcrossed to C57BL/6J or 129/SvImJ mice to maintain independent lines on both genetic backgrounds. Two 3′ primers, located downstream of the insertion site in intron 19 (R2) and at the 3′ end of the pGT0lxr targeting vector sequence (V13), were combined with a 5′ primer upstream of the insertion site (F3), to generate a three-primer PCR yielding different-sized products from the WT (274 bp) and targeted alleles (235 bp) that are resolved by 2% (wt/vol) agarose gel electrophoresis. Primer sequences are listed in Table S1. A second ES clone (in the C57BL/6J background), which contains a gene-trap insertion in intron 4 of the *Sec23b* gene and floxed exons 5 and 6 (Fig. S6), was obtained from the International Knockout Mouse Consortium. These ES cells were expanded and injected into C57BL/6J blastocysts by the transgenic and targeting facility at Case Western Reserve University. Matings between chimeric founder males and C57BL/6J females produced offspring with germ-line transmission of the mutant allele in the pure C57BL/6J background. The floxed exons were deleted by mating with an EIIa-cre mouse (stock no. 003314; The Jackson Laboratory). All mice had free access to food and water and were kept in cages in a 12-h light/dark cycle. All animal experimental protocols were approved by the Institutional Animal Care and Use Committees at the University of Michigan and the Cleveland Clinic Foundation.

Animal Procedures. Timed matings were performed as previously described (43). The morning after copulation plug was observed is designated as E0.5. Tissues were dissected from embryos harvested at different embryonic days. Blood was collected by using heparin-coated collection tubes from decapitated live-born neonates anesthetized with isoflurane. Blood glucose levels were measured using the Contour Blood Glucose Monitoring System (Bayer). The complete blood count was determined in an Advia120 whole blood analyzer (Bayer).

Antibodies. Rabbit polyclonal anti-SEC23A and SEC23B antibodies were generated against synthetic peptides (SEC23A, CQKFGEYHKDDPNSFRFSET and DNAKYVKKGTKHFEA; SEC23B, LTKSAMPVQQARPAQPQEQP and KFGQYNKEDPTSFRLSDS). Other antibodies used in the study are listed in Table S2.

RNA Extraction and Real-Time PCR. Tissues were dissected from embryos in cold PBS solution and immediately transferred to RNAlater (Ambion) for storage. After genotyping, total RNA was isolated by using a PureLink RNA Micro Kit (Invitrogen). Reverse transcription was performed with the iScript cDNA Synthesis Kit (Bio-Rad). The iQ SYBR Green Supermix (Bio-Rad) was used for quantitative RT-PCR in a CFX384 Real Time Thermalcycler (Bio-Rad). For each primer pair, amplification efficiency was confirmed to be near 100%. Relative gene expression was calculated by the $2^{-\Delta Ct}$ method using *Gapdh* or *Atcb* (β-actin) as reference genes according to manufacturer instructions.

EM and Immuno-EM. Isolated pancreatic and salivary gland tissues were immediately fixed in 2.5% (wt/vol) glutaraldehyde and 4% (wt/vol) formaldehyde, pH 7.3, for 24 h, followed by postfixation with 1% (wt/vol) osmium tetroxide for 1 h. After en bloc staining and dehydration with ethanol, samples were embedded in Eponate 12 medium (Ted Pella). Ultrathin sections (85 nm) were stained with uranyl acetate and lead citrate and examined on a Philips CM12 electron microscope operated at 60 kv. To count the numbers of zymogen granules in salivary glands, we randomly chose 20 acini from each genotype containing ∼200 cells.

For immuno-EM analysis, samples were fixed in 4% (wt/vol) formaldehyde, 0.05% glutaraldehyde in 0.1 M phosphate buffer, dehydrated, and embedded in LR White medium (Ted Pella). Ultrathin sections were mounted on Formvar carbon-coated nickel grids (Ted Pella) and incubated with primary antibody overnight before 45 min incubation with 10 nm gold-conjugated goat anti-rabbit IgG (Ted Pella). Grids were then stained with uranyl acetate and lead citrate and observed in a CM-12 electron microscope (Philips). To determine the total number of glucagon-positive cells, the whole thin sections of two independent *Sec23b*$^{gt/gt}$ dorsal pancreata were thoroughly examined. Glucagon-positive cells from a random field of ∼10% area of the WT sections were counted to estimate the total number of α-cells in a whole dorsal pancreas section.

Immunofluorescence Imaging and β-Gal and TUNEL Staining of Cryosections. Isolated tissues were fixed in 4% (wt/vol) paraformaldehyde at 4 °C. After equilibration in 30% (wt/vol) sucrose in 1× PBS solution, tissues were embedded in optimal cutting temperature compound (Sakura Finetek) and frozen on dry ice. Cryosections (6 μm) were stained with H&E for histological analysis. Immunofluorescence staining was performed on PFA-fixed cryosections as described previously (44). TUNEL staining was performed according to the manufacturer's instructions (Roche Diagnostics). X-gal staining for β-gal activity and immunofluorescence staining of MEFs were performed as previously described (43). Images were visualized and captured with an Olympus FluoView confocal microscope.

Alcian Blue and Alizarin Red Staining. Newborn pups were euthanized, skinned, eviscerated, and then fixed in 95% (vol/vol) ethanol for 3 d. Samples were stained in Alcian blue solution (0.015% Alcian blue in 95% (vol/vol) ethanol/20% (vol/vol) glacial acetic acid) for 24 h, followed by two washes in 95% (vol/vol) ethanol (24 h each), then cleared in 1% (wt/vol) KOH for 5 h before being incubated in alizarin red solution (0.005% alizarin red in 1% KOH) overnight. Samples were finally soaked in 1% KOH/20% (vol/vol) glycerol for 2 d until clear, and then placed in a 1:1 mixture of glycerol and ethanol for storage.

SEC23A and SEC23B Expression Plasmid Construction. To express GFP-SEC23A and GFP-SEC23B fusion proteins, full-length cDNAs for *Sec23a* and *Sec23b* were amplified by PCR by using a cDNA library from murine 3T3-L1 adipocytes (45) as template with the following primer pairs (Table S1): Sec23a-XhoI and Sec23a-BamHI and Sec23b-XhoI and Sec23b-BclI. The PCR products were subsequently double-digested with XhoI/BamHI or XhoI/BclI, respectively, and cloned in-frame into the pEGFP-C3 vector (BD Bioscience) by using XhoI and BamHI sites. The expression constructs were confirmed by direct DNA sequencing.

Comparison of SEC23A and SEC23B Protein Expression. COS1 cells were cultured in DMEM supplemented with 10% (vol/vol) FBS and transfected with plasmids expressing GFP-SEC23A or GFP-SEC23B fusion proteins. Cells were lysed with Nonidet P-40 buffer (44), and the total protein levels were quantified by using the Bradford assay (Bio-Rad). To compare the amounts of SEC23A and SEC23B fusion proteins, we first performed standard Western blot analyses on serial dilutions of cell lysates by using antibodies against GFP and β-actin. The bands with similar intensities as quantified by using ImageJ software (National Institutes of Health) represent similar amounts of GFP fusion proteins. Equal amounts of GFP-SEC23A and GFP-SEC23B proteins, along with lysates from different mouse embryonic tissues or cell lines, were further subjected to immunoblotting by using specific antibodies against SEC23A and SEC23B. The relative efficiencies of the SEC23A and SEC23B antibodies were determined by comparing the band intensities of the GFP-SEC23A and GFP-SEC23B fusion proteins. Data were normalized to β-actin. The relative expressions of the two SEC23 paralogues in the same tissues and cells were estimated by dividing the normalized band intensities for SEC23A and SEC23B in each tissue or cell line.

Statistical Analysis. Student *t* test was used to assess the significance of differences between two groups of data ($P < 0.05$ is deemed significant). The chi-squared test was used to evaluate the significance of difference between the expected and observed genotype distributions.

ACKNOWLEDGMENTS. This work was supported by in part by National Institutes of Health (NIH) Grants R01 HL094505 (to B.Z.), R01 HL039693 (to D.G.), and P01-HL057346 (to D.G.), and the Chicago Diabetes Project (S.A and J.J.). The Transgenic Animal Model Core of the University of Michigan was supported by NIH Grants AR20557 and P30AG013283 and the University of Michigan Center for Organogenesis. D.G. is an investigator of the Howard Hughes Medical Institute.

1. Bonifacino JS, Glick BS (2004) The mechanisms of vesicle budding and fusion. *Cell* 116: 153–166.
2. Gürkan C, Stagg SM, Lapointe P, Balch WE (2006) The COPII cage: Unifying principles of vesicle coat assembly. *Nat Rev Mol Cell Biol* 7:727–738.
3. Jensen D, Schekman R (2011) COPII-mediated vesicle formation at a glance. *J Cell Sci* 124:1–4.
4. Lee MC, Miller EA, Goldberg J, Orci L, Schekman R (2004) Bi-directional protein transport between the ER and Golgi. *Annu Rev Cell Dev Biol* 20:87–123.
5. Barlowe C, et al. (1994) COPII: A membrane coat formed by Sec proteins that drive vesicle budding from the endoplasmic reticulum. *Cell* 77:895–907.
6. Lee MC, Miller EA (2007) Molecular mechanisms of COPII vesicle formation. *Semin Cell Dev Biol* 18:424–434.
7. Miller E, Antonny B, Hamamoto S, Schekman R (2002) Cargo selection into COPII vesicles is driven by the Sec24p subunit. *EMBO J* 21:6105–6113.
8. Miller EA, et al. (2003) Multiple cargo binding sites on the COPII subunit Sec24p ensure capture of diverse membrane proteins into transport vesicles. *Cell* 114:497–509.

9. Aridor M, Weissman J, Bannykh S, Nuoffer C, Balch WE (1998) Cargo selection by the COPII budding machinery during export from the ER. *J Cell Biol* 141:61–70.
10. Mancias JD, Goldberg J (2007) The transport signal on Sec22 for packaging into COPII-coated vesicles is a conformational epitope. *Mol Cell* 26:403–414.
11. Fromme JC, Orci L, Schekman R (2008) Coordination of COPII vesicle trafficking by Sec23. *Trends Cell Biol* 18:330–336.
12. Fath S, Mancias JD, Bi X, Goldberg J (2007) Structure and organization of coat proteins in the COPII cage. *Cell* 129:1325–1336.
13. Stagg SM, et al. (2008) Structural basis for cargo regulation of COPII coat assembly. *Cell* 134:474–484.
14. Cai H, et al. (2007) TRAPPI tethers COPII vesicles by binding the coat subunit Sec23. *Nature* 445:941–944.
15. Watson P, Forster R, Palmer KJ, Pepperkok R, Stephens DJ (2005) Coupling of ER exit to microtubules through direct interaction of COPII with dynactin. *Nat Cell Biol* 7: 48–55.
16. Lord C, et al. (2011) Sequential interactions with Sec23 control the direction of vesicle traffic. *Nature* 473:181–186.
17. Boyadjiev SA, et al. (2011) Cranio-lenticulo-sutural dysplasia associated with defects in collagen secretion. *Clin Genet* 80:169–176.
18. Boyadjiev SA, et al. (2006) Cranio-lenticulo-sutural dysplasia is caused by a SEC23A mutation leading to abnormal endoplasmic-reticulum-to-Golgi trafficking. *Nat Genet* 38:1192–1197.
19. Fromme JC, et al. (2007) The genetic basis of a craniofacial disease provides insight into COPII coat assembly. *Dev Cell* 13:623–634.
20. Bianchi P, et al. (2009) Congenital dyserythropoietic anemia type II (CDAII) is caused by mutations in the SEC23B gene. *Hum Mutat* 30:1292–1298.
21. Schwarz K, et al. (2009) Mutations affecting the secretory COPII coat component SEC23B cause congenital dyserythropoietic anemia type II. *Nat Genet* 41:936–940.
22. Scheuner D, et al. (2001) Translational control is required for the unfolded protein response and in vivo glucose homeostasis. *Mol Cell* 7:1165–1176.
23. Lang MR, Lapierre LA, Frotscher M, Goldenring JR, Knapik EW (2006) Secretory COPII coat component Sec23a is essential for craniofacial chondrocyte maturation. *Nat Genet* 38:1198–1203.
24. Zhou Q, et al. (2007) A multipotent progenitor domain guides pancreatic organogenesis. *Dev Cell* 13:103–114.
25. Hald J, et al. (2008) Generation and characterization of Ptf1a antiserum and localization of Ptf1a in relation to Nkx6.1 and Pdx1 during the earliest stages of mouse pancreas development. *J Histochem Cytochem* 56:587–595.
26. Schaffer AE, Freude KK, Nelson SB, Sander M (2010) Nkx6 transcription factors and Ptf1a function as antagonistic lineage determinants in multipotent pancreatic progenitors. *Dev Cell* 18:1022–1029.
27. Gradwohl G, Dierich A, LeMeur M, Guillemot F (2000) neurogenin3 is required for the development of the four endocrine cell lineages of the pancreas. *Proc Natl Acad Sci USA* 97:1607–1611.
28. Gu GQ, Dubauskaite J, Melton DA (2002) Direct evidence for the pancreatic lineage: NGN3+ cells are islet progenitors and are distinct from duct progenitors. *Development* 129:2447–2457.
29. Westrick RJ, et al. (2010) Spontaneous Irs1 passenger mutation linked to a gene-targeted SerpinB2 allele. *Proc Natl Acad Sci USA* 107:16904–16909.
30. Rutkowski DT, Kaufman RJ (2007) That which does not kill me makes me stronger: Adapting to chronic ER stress. *Trends Biochem Sci* 32:469–476.
31. Walter P, Ron D (2011) The unfolded protein response: From stress pathway to homeostatic regulation. *Science* 334:1081–1086.
32. Jonsson J, Carlsson L, Edlund T, Edlund H (1994) Insulin-promoter-factor 1 is required for pancreas development in mice. *Nature* 371:606–609.
33. Bi X, Corpina RA, Goldberg J (2002) Structure of the Sec23/24-Sar1 pre-budding complex of the COPII vesicle coat. *Nature* 419:271–277.
34. Russo R, et al. (2010) Mutational spectrum in congenital dyserythropoietic anemia type II: Identification of 19 novel variants in SEC23B gene. *Am J Hematol* 85:915–920.
35. Iolascon A, et al. (2010) Molecular analysis of 42 patients with congenital dyserythropoietic anemia type II: new mutations in the SEC23B gene and a search for a genotype-phenotype relationship. *Haematologica* 95:708–715.
36. Kaiser CA, Schekman R (1990) Distinct sets of SEC genes govern transport vesicle formation and fusion early in the secretory pathway. *Cell* 61:723–733.
37. Jones B, et al. (2003) Mutations in a Sar1 GTPase of COPII vesicles are associated with lipid absorption disorders. *Nat Genet* 34:29–31.
38. Roberts B, Clucas C, Johnstone IL (2003) Loss of SEC-23 in Caenorhabditis elegans causes defects in oogenesis, morphogenesis, and extracellular matrix secretion. *Mol Biol Cell* 14:4414–4426.
39. Lee AH, Chu GC, Iwakoshi NN, Glimcher LH (2005) XBP-1 is required for biogenesis of cellular secretory machinery of exocrine glands. *EMBO J* 24:4368–4380.
40. Pandol SJ, Gorelick FS, Lugea A (2011) Environmental and genetic stressors and the unfolded protein response in exocrine pancreatic function - a hypothesis. *Front Physiol* 2:8.
41. Witt H, Apte MV, Keim V, Wilson JS (2007) Chronic pancreatitis: Challenges and advances in pathogenesis, genetics, diagnosis, and therapy. *Gastroenterology* 132: 1557–1573.
42. Szmola R, Sahin-Tóth M (2010) Pancreatitis-associated chymotrypsinogen C (CTRC) mutant elicits endoplasmic reticulum stress in pancreatic acinar cells. *Gut* 59:365–372.
43. Zhang B, et al. (2011) Mice deficient in LMAN1 exhibit FV and FVIII deficiencies and liver accumulation of α1-antitrypsin. *Blood* 118:3384–3391.
44. Zheng C, Liu HH, Yuan S, Zhou J, Zhang B (2010) Molecular basis of LMAN1 in coordinating LMAN1-MCFD2 cargo receptor formation and ER-to-Golgi transport of FV/FVIII. *Blood* 116:5698–5706.
45. Ribon V, Printen JA, Hoffman NG, Kay BK, Saltiel AR (1998) A novel, multifuntional c-Cbl binding protein in insulin receptor signaling in 3T3-L1 adipocytes. *Mol Cell Biol* 18: 872–879.